ORIGINAL ARTICLE

Land subsidence assessment under excessive groundwater pumping using ESA Sentinel-1 satellite data: a case study of Konya Basin, Turkey

Hande Mahide Yeşilmaden[1,2] · Çağrı Alperen İnan[1,3] · Bedri Kurtuluş[1,4] · Mustafa Can Canoğlu[5,6] · Özgür Avşar[1] · Moumtaz Razack[6]

Abstract

Land subsidence analysis using satellite imagery is a consequential subject. Earth scientists have begun utilizing satellite imagery as an alternative to in-situ measurements and conceptual models. Synthetic aperture radar (SAR) images, moreover, utilize the reformer approach more than traditional satellite imagery with the use of high-resolution radar images. As a natural hazard, land subsidence is mostly attributed to excessive groundwater extraction, which is also the main reason for choosing the Konya Plain in Turkey as the study area for the present work. Since the Konya region is an agricultural and industrial land, groundwater extraction has been a challenging circumstance for the last few years. Change in groundwater level is also correlated with land subsidence rates through hydrogeological conceptualization. In this study, SAR images of the Sentinel 1 satellite are utilized for land subsidence rate calculation with the European Space Agency's SNAP software. Differential SAR interferometry (DInSAR) technique was used, which makes possible to detect deformation on the ground surface of the same portion of the Earth's surface using SAR images. The different acquisitions with DInSAR method allow to create differential interferograms that provide information ground motion with accuracy in cm. Three periods were utilized as 2016–2017, 2017–2018 and 2018–2019 the mean land subsidence rates were calculated for each period as 2.2, 1.4 and 1.7 cm/year, respectively. In the sum of the 3-year period, the maximum subsidence value went up to 16 cm.

Keywords Sentinel 1 · SAR · Land subsidence · ESA · Differential interferometry · DInSAR

Introduction

The term land subsidence is defined as sudden and/or gradual settlement of the ground. It may occur due to natural or artificial movement of subsurface materials such as natural consolidation of sediments, excess groundwater extraction, tectonic forces, and construction load in urbanized areas. Land subsidence can cause a loss of life as well as severe property losses regardless of its extent. Increasing demand for water in industrialized metropolitans and excess water

✉ Hande Mahide Yeşilmaden
hande-mahide.yesilmaden@etu.u-bordeaux-montaigne.fr

Çağrı Alperen İnan
cagri-alperen.inan@mines-ales.fr

Bedri Kurtuluş
bedri.kurtulus@kfupm.edu.sa

Mustafa Can Canoğlu
mccanoglu@sinop.edu.tr

Özgür Avşar
ozguravsar@mu.edu.tr

Moumtaz Razack
moumtaz.razack@univ-poitiers.fr

[1] Department of Geological Engineering, Muğla Sıtkı Koçman University, Menteşe, TR48000 Muğla, Turkey

[2] Sciences et Technologies (Terre, Eau, Image), EA 4592 Géoressources et Environnement, Université Bordeaux Montaigne, FR33607 Pessac, France

[3] Centre de Recherche et d'enseignement en Environnement et en Risques, IMT Mines Alès, 1 Rue Jules Renard, 30100 Alès, France

[4] The Center of Membranes and Water Security, King Fahd University of Petroleum and Minerals, Dhahran, Kingdom of Saudi Arabia

[5] Environmental Engineering Department, Sinop University, TR57000 Sinop, Turkey

[6] Department of Hydrogeology, University of Poitiers, IC2MP, UMR CNRS 7258, 86073 Poitiers Cedex, France

extraction have also proven to be major causes of land subsidence over the last few decades (Kontogianni et al. 2006; Teatini et al. 2006; Lofgren 1969). Previous studies have highlighted the importance of this subject for those regions vulnerable to land subsidence due to groundwater withdrawal. It became important to estimate the rate of subsidence in urbanized and agricultural areas; especially where compressible aquifer systems exist in arid to semi-arid regions with high water demand (Kontogianni et al. 2006; Teatini et al. 2006,2005; Lofgren 1969; Widodo et al. 2019; Perski 2003; Carbognin et al. 2004; Çomut et al. 2016; Imamoglu et al. 2019; Xue et al. 2005; Motagh et al. 2007; Holzer and Johnson 1985).

Together with the need for scientific focus on the subject, enhancements in remote sensing methods have increased the reliability of land monitoring (Ferretti et al. 2007; Yague-Martinez et al. 2016; Prats-Iraola et al. 2012; Veci 2015). Remote sensing tools, particularly Synthetic aperture radar data from different satellites, have been utilized in studies for detecting deformations on land [i.e., ERS-1, ERS-2, Envisat, Sentinel-1 (European Space Agency, ESA); ALOS-1, ALOS-2 (Japan Aerospace Exploration Agency, JASA); TerraSAR-X,TanDEM-X (German Aerospace Center, DLR); COSMO-Skymed (Italian Space Agency, ASI)]. These SAR satellites employ predetermined frequencies, and the predominant wavelengths are on C, L, and X-bands. Sentinel-1 (ESA) has made substantial progress in land monitoring working on its C-band, reducing the revisit time to 12 days, obtaining higher spatial resolution (up to 5×20 m in wide swath interferometric acquisition mode) compared to its former satellites, and having the ability to monitor over cloud cover or during storms (Schubert et al. 2015; Elachi et al. 1982). Sentinel-1 revealed an open access Level-1 Single Look Complex (SLC), having geo-referenced findings with phase information, and ground range detected (GRD) projected onto the ground, and multi-look products having amplitude information. SLC terrain observation with progressive scan SAR (TOPSAR) was used as the replacement acquisition mode, scanning synthetic aperture radar SCANSAR with reduced azimuth resolution, and scalloping effects, yielding the synchronized bursts between each pass providing a better interferometric pair alignment (Guccione 2006). TOPS acquisition mode and TOPSAR technique, which are currently being developed and integrated into ESA's open-source software SNAP, provide an opportunity for robust solutions for interferometric analysis (User Guides—Sentinel-1 SAR 2020).

This paper aimed to investigate land subsidence by means of SAR images and using a differential interferometry method coupled with hydrogeological conceptualization at Konya basin, and to compare the subsidence rates with land cover properties and piezometric levels to point out the effects of land cover and groundwater on land subsidence.

Study area

Konya city is in central Anatolian Turkey located between the Taurus mountain in the south; the Salt Lake in the north; Isparta and Afyon in the west, and Niğde and Aksaray cities in the east (Fig. 1). The study area is limited by alluvium and the quality of the satellite images. The low overlapping bursts of the SAR image for selected dates have been removed from the alluvium and the shape of study area created.

Konya is Turkey's largest city in terms of land area, and the seventh largest city based on population records. The reason Konya was chosen as the study area is that it has been facing serious land subsidence problems for the last 2 decades. As Konya is a growing agricultural and industrial city, water demand and extraction rate have created a serious need for stress-relief under the ground because of excess groundwater extraction, and consolidation of sediment in the quaternary deposits in the Konya basin (Bayari et al. 2008b). The meteorological records show that Konya is a semi-arid region where incoming water supply cannot meet the demand in the region: this leads to excess groundwater demand, decreasing the water table level in populated and agricultural areas where confining units and alluvium cannot manage the artificial loads and subsidence becomes inevitable (Çomut et al. 2016; Aksoy 2019).

Geological setting and hydrogeological situation of the study area

Determination of the geological condition of the study area is very important for deciding the method to be utilized in land subsidence rate estimation. In the study area and nearby environs, Cenozoic and Mesozoic aged geological units can be observed. Mesozoic limestone underlies the base of the stratigraphic section. This unit is covered unconformably by the Paleogene series (carbonates, conglomerates, shale, sandstone, siltstone). Neogene carbonates cover the Paleogene series conformably. Finally, Quaternary-age alluviums cover all these geological units unconformably and the volcanic units (Miocene-Quaternary) locally cross the alluviums. The geological structure around the Konya Closed Basin (KCB) is represented by three structural blocks; Tauride-Anatolide Block (TAB), Sakarya Zone Block, (SZB) and Kirsehir Massive Block (KMB). The stratigraphy of the Konya Closed Basin can be defined by; (1) the content of TAB being clastic rock from Paleozoic to late Mesozoic, a massive body of ophiolite and ophiolitic melange (Okay and Tüysüz 1999) (2) the SZB comprised Triassic to Jurassic clastics, carbonates

Fig. 1 Location map of study area

from Jurassic to Cretaceous, clastic and volcanic units from middle-late Cretaceous and Paleogene carbonates and clastics (3) the characteristic content of KMB is metamorphic units and voluminous granitic rocks which are aged Cretaceous. The Paleogene series of TAB and SZB show similarities and mainly include conglomerates, shale, sandstone, siltstone, and marine carbonates (Dirik and Göncüoglu 1996) where they are covered by paleo lake sediments and alluvial fans (Okay and Tüysüz 1999; Afşin et al. 2012). The dissolution of Neogene carbonates resulting from the neotectonics of Central Anatolia are the key reason for internal karstification, since volcanic and acidic gasses in groundwater continuously dissolve limestone (Canik and Çörekçioğlu 1985). The term 'Obruk' is an internationally recognized Turkish geomorphic term identifying the collapse of dolines which can be generally observed in the Konya Closed Basin (KCB) in central Turkey (Bayari et al. 2008b). The Central Anatolian extensional regime has strongly impacted the current geomorphology of Konya basin, along with the E–W and NW–SE oriented horst—graben systems since Middle Miocene (Kocyigit, 2005). Hereby, this might lead to exposure of the land subsidence and Obruk formations, which are related by tectonism, as well as the effects of water extraction in the region. Obruk formations have been

attributed to dissolution of Neogene carbonates since Miocene. The Konya Sub Basin, a part of Konya Closed Basin, comprises a Neogene aquifer to meet its need for water (Canik and Çörekçioğlu 1985; Okay and Tüysüz 1999; Bayari et al. 2008a).

There are three main aquifers in the study area and nearby environs. Mainly, TAB, SZB and volcanic units, and the main aquifers are represented by these units (modified from Özyurt et al. 2018). TAB and SZB are the main individual aquifers of KCB. Moreover, the Paleogene unit which covers unconformably the Mesozoic limestones and Plio-Quaternary sediments (alluvium) acts as aquitard systems. Plio-Quaternary aged alluviums are generally formed by clayey and silty sands which have low-hydraulic conductivity restricting the vertical groundwater flow. Although it has low-hydraulic conductivity, horizontal flow can be observed in Plio-Quaternary units. Neogene and SZB aquifers are separated by the Paleogene aquitard. The Neogene aquifer, composed of limestone, controls formation, and productive fresh-water storage. The lowermost confined aquifer, which is a deep thermal aquifer with saline groundwater, is called the TAB aquifer. Both consist of Paleozoic–Mesozoic karstic carbonates (Bayari et al. 2008a). In the Neogene aquifer and the TAB of the Konya closed basin, karst formations are well developed. The shallow Neogene aquifer shows confined and

unconfined conditions where it is covered by quaternary sediments and by Obruk plateau, respectively (Aksoy 2019; Özyurt et al. 2018). The main groundwater flow recharge comes from the Taurus mountains to the Salt Lake through the shallow and deep flow paths. The conceptional hydrogeological model shows that the groundwater flow in the Plio-Quaternary alluvium unit is mainly from south to north, and partly south-east to north-west based on the hydraulic head distribution of the late 1960's, and piezometric levels presented in the present work in Figs. 2, 4 (modified from Bayari et al. 2008b).

Decline in ground water level, shown in Fig. 3, from 1968 to 2018 is considered the biggest cause of land subsidence. The groundwater level decline average for study area is 30 m according to data taken from the General Directorate of State Hydraulic Works of Turkey based on 12 wells for 1968, and 144 wells for 2018. As shown in the cross-section A–A', the groundwater table was mostly in the Plio-Quaternary layers in 1968, within the study area, whereas resulting

decline reached the groundwater table at various units such as Miocene Volcanics, Neogene aquifer and Mesozoic limestones (Fig. 2). The stress-relief resulting from fluid pressure decline following water table decline, is compensated for by an over-load of pressure causing land subsidence by compaction in Plio-Quaternary sediments, representing upper unconfined aquifer layers and the lower confined Neogene aquifer, which is confined by aquitard levels as a result of pressure decrease in the aquifer.

Since the frame of presented study is to create a methodology for calculating subsidence through time series remote sensing data, comparing in-situ measurements with our subsidence estimations would be an enrichment for the performance of the present study. GNSS observations concluding a subsidence of 12 mm/year and 52 mm/year in the west and northwest section of Konya closed basin where the intense groundwater drilling wells and neighborhoods are mostly found for a period of 3 years (Ustun et al. 2010; Üstün et al. 2015). In the presented
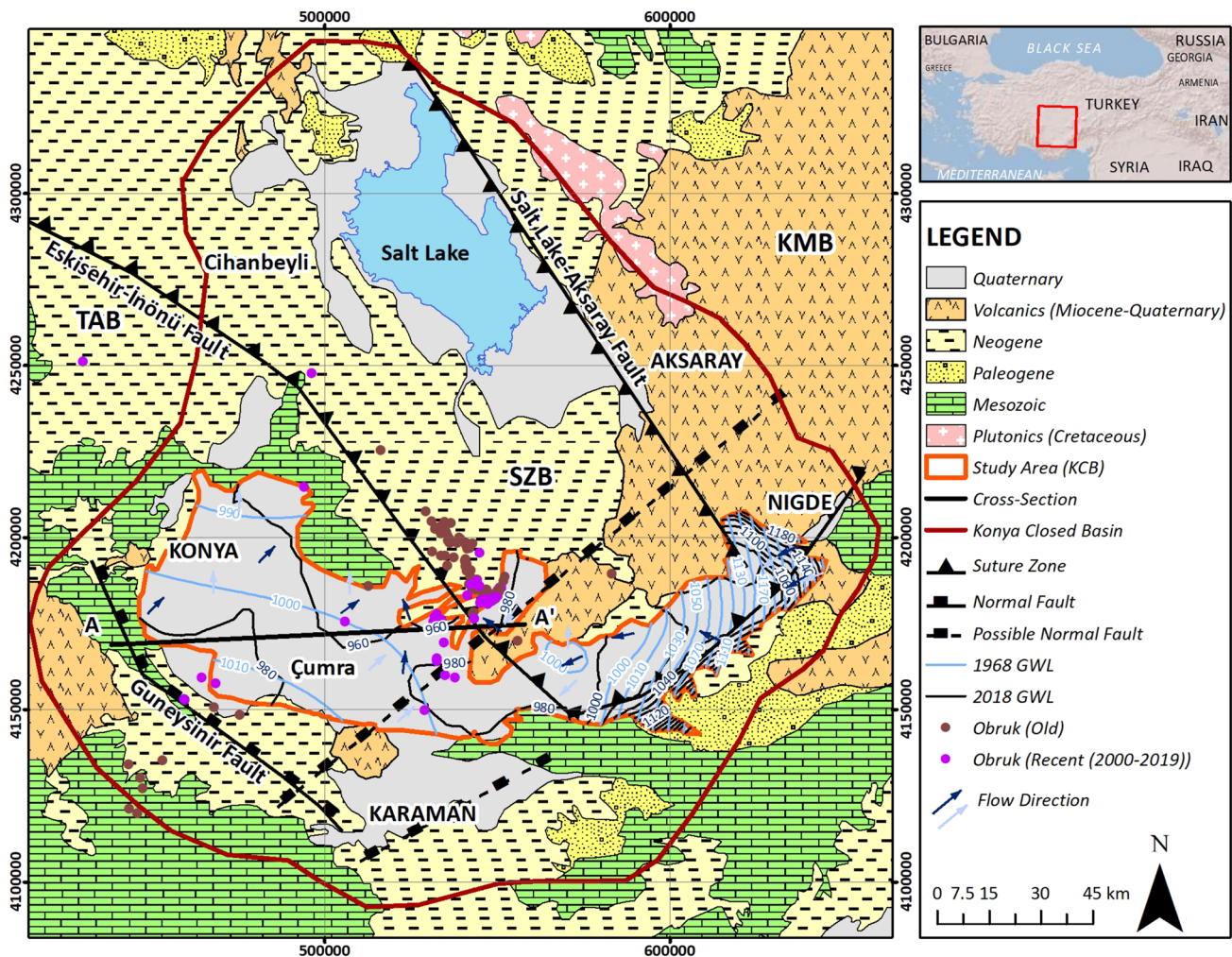

Fig. 2 Geological map of the study area and nearby environs (modified from Özyurt et al. 2018)
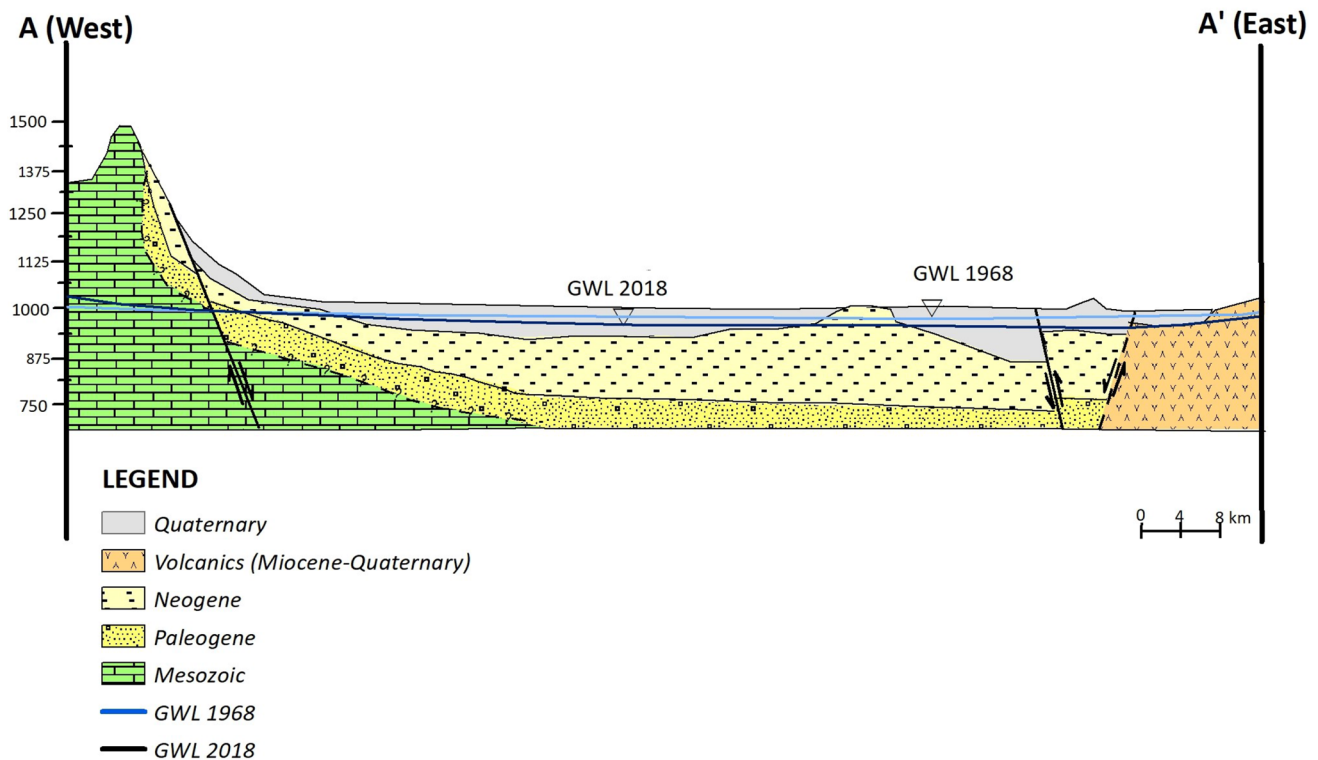
Fig. 3 Geological cross-section (modified from Özyurt et al. 2018)

study, land subsidence rate will be proposed via satellite interferometry for a different period of 3 years which could be an evidence the increase in the rate of land subsidence caused by increased groundwater extraction and depleted groundwater level which will be proved by ground water level estimations through Geographic Information System (GIS) based groundwater level monitoring.

Annual mean decline in the head has been recorded at 1 m/year in several regions since 1980, according to groundwater research (Bayari et al. 2008b; Doğdu et al. 2007; Ozdemir 2015). Studies done by the General Directorate of State Hydraulic Works of Turkey prove the severity of water table decline, recording 20–25 m displacement in most of the wells between the early 70 s and 2009, located in the middle of the Konya sub-basin near Hotamis and Karapinar plains (Doğdu et al. 2007; Ozdemir 2015; Doğan and Yılmaz 2011). When the aquifer thicknesses and piezometric levels are considered, where the thickness of Plio-Quaternary units vary from 0 to 250 m in depth, and the bottom of the Neogene aquifer reaches 650 m in depth, groundwater extractions have decreased the water table from the upper most aquifer to Neogene aquifer, nearly 965 m from sea level. This shows a drastic decrease in the groundwater level reaching approximately 30 m from 1968 to 2018 (Figs. 3, 4). Between 2009 and 2018, there has been an up to 15-m decrease in groundwater level.

As a natural result of this decline, land subsidence has become a critical issue in the region. Considering hydrogeological conceptualization of the study area, and land subsidence findings from previous studies; Neogene units are exposed to subsidence by the dramatic decline in aquifer pressure (Fig. 2). There is also a horizontal hydraulic continuity between the Paleogene–Neogene units and Mesozoic limestone, also Miocene–Quaternary Volcanics.

Through the south of Konya closed basin, carbonate units are covered by clay, silt, sand and marl which is sometimes uncompacted. These formations cannot support the above over-load pressure following groundwater decline (Canik and Çörekçioğlu 1985; Ozdemir 2015). When previously mentioned facts about the hydrogeology of the region are considered, they are likely to show that extreme water extraction is interrelated with shrinkage of confining rock or sediment units, and partly regional extensional regime is causing land subsidence in the Konya basin (Yilmaz 2010).

Data collection

In this study, however, there has been substantial investigation aiming to understand the extent of groundwater extraction and land subsidence, the scientific resolution of these works leads us to consider combining hydrogeological
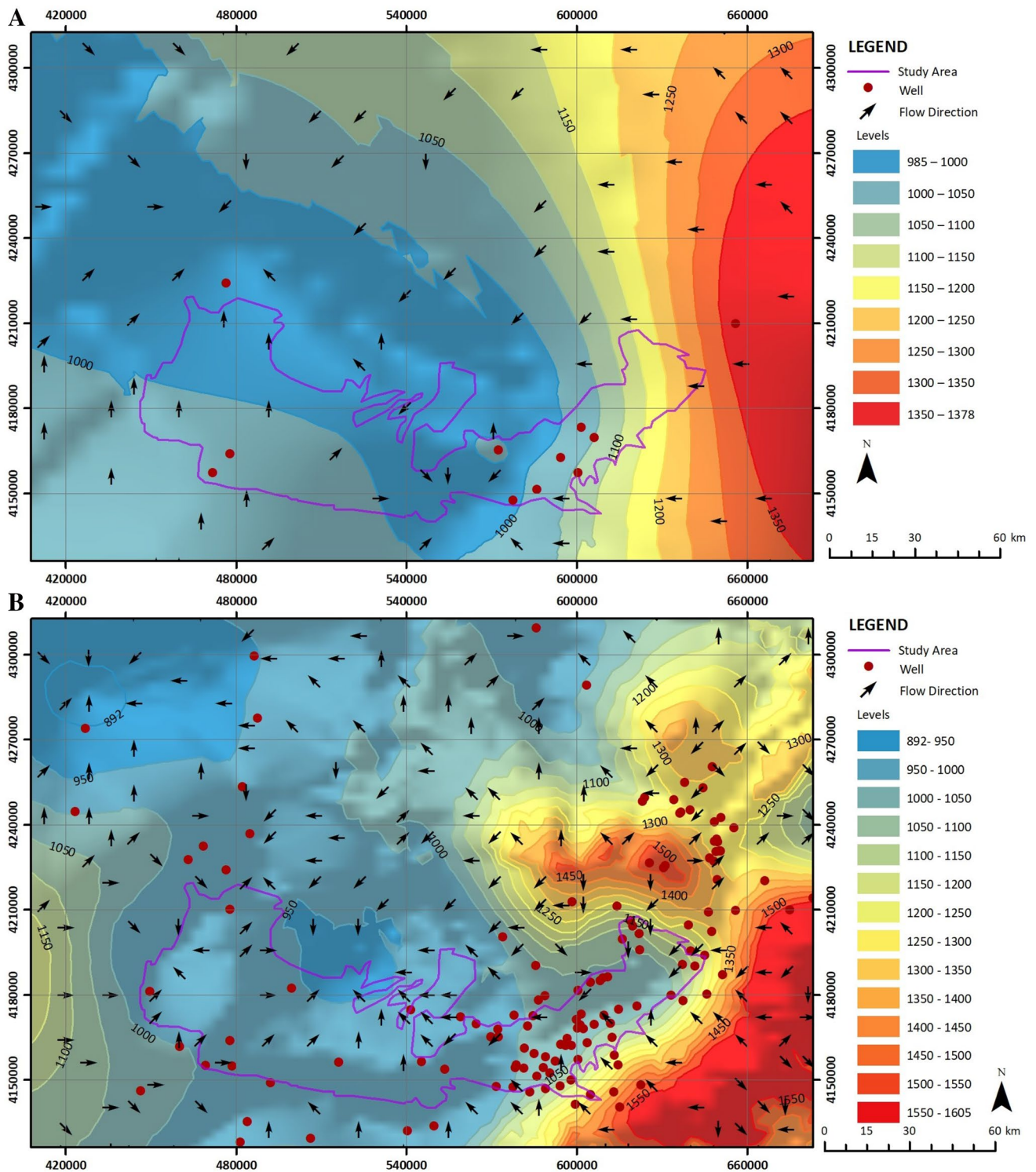
Fig. 4 Piezometric maps for 1968 (**A**) and 2018 (**B**), respectively

findings with remote sensing information. Therefore, Level-1 SLC products from the Sentinel-1 satellite for the years 2016–2019 were used to perform interferometry analysis on the Konya sub-basin to reveal the annual land subsidence rate. Satellite information and in-situ measurements will be correlated to inspire further hybrid studies on the subject, which will be a powerful tool for future land subsidence work. For groundwater monitoring, groundwater

well data from 1968 to 2018 is provided by the archives of Turkish Hydraulic State for the study.

Methodology

Groundwater level monitoring

Groundwater levels from the sea level are computed with Gaussian process regression interpolation method for the years 1968 and 2018 in geographic information system environment. So that, it is possible to observe the overall change in groundwater for 40 years of period and for reasoning the land subsidence in the Konya region for the reference years where we have satellite data.

Remote sensing approach

Researches have showed relevance of satellite imagery on the land deformation monitoring and land subsidence studies. Sentinel-1 mission is a radar imaging system, which is a section of the European Union's Copernicus program. It includes two satellite constellations; Sentinel-1A and Sentinel-1B. Both are in a near-polar, sun-synchronous orbit and with a 12-day cycle (Crosetto et al. 2005; Jiang et al. 2011; Potin et al. 2015). The satellites were launched in April 2014, and the data release started in October 2014. Sentinel-1 carries a synthetic aperture radar (SAR) and includes C-band (User Guides—Sentinel-1 SAR 2020). This radar instrument is an active system so provides a series of data in all-weather conditions, and at any time of the day or night. The Sentinel-1A radar can operate on several modes including interferometric wide swath (IW), extra wide swath (EW), wave (WV), and strip map (SM) (Data Products 2020). Three sub swathes were captured; IW1, IW2, and IW3, using terrain observation with progressive scans SAR (TOPSAR). The data processing products are Level-0, Level-1 single look complex (SLC), Level-1 ground range detected (GRD), and Level-2 IW, the SLC product includes three–six images which refer to one image per sub-swath and per polarization channel (Zan and Guarnieri 2006). In this study, Sentinel 1A SLC IW (descending) images from 2016 to 2019 are used (Table 1).

The open-source software of ESA, so-called Sentinel application platform (SNAP), is used to implement the methodology. SNAP has special toolboxes for Sentinel-1 SAR image processing. The graph processing tool (GPT) of SNAP is used to combine tools to perform operations consistently. SAR is a microwave imaging system. SAR with interferometric configuration, so-called interferometric synthetic aperture radar (InSAR), ensures accurate measurements of the radiation travel path due to its coherence (Ferretti et al. 2007).

SAR signals contain amplitude and phase information about the microwave field backscattered by several scatters corresponding with the resolution. The amplitude can be explained by the strength of the radar response and depends on the chemical composition of the scatters on the terrain. Phase is determined by the distance between satellite and ground target. InSAR exploits the phase difference between two SAR observations and extracts the information about ground deformation. The phase of coregistered images taken at two different times are combined to create an interferogram that is highly correlated to the terrain topography (Ferretti et al. 2007). One of the most important InSAR applications is differential interferometry (DInSAR), which is the method adopted to calculate the subsidence of the Konya Plain. Knowing that Sentinel SAR imagery have faced difficulties while penetrating vegetated areas mentioned in several articles in the literature coherence mask applied in pre-interferometry period. The coherence threshold for the interferograms is chosen as 0.25 to find coherent pixels; where 0 coherence indicates a total noise by the vegetation interference (Cigna et al. 2004; Osmanoglu et al. 2015; Sowter et al. 2016).

Determination of subsidence is implemented in three main steps built with GPT (Fig. 5). The input data are Sentinel 1A IW SLC production downloaded from the Copernicus Open Access Hub. The downloaded IW SLC products contain one image, one per polarization channel, and one per sub-swath. With preference given to single polarization, there will be horizontal ensuing of three images in an IW product. Each sub-swath image includes a series of bursts, and each burst has been processed as an individual SLC image. In the first GPT model, for interferometric processing, master and slave images are coregistered into a stack. In this way, the pixels in the slave image are moved and aligned in coherence with the master image. The pair composed of the master and the slave image; therefore, show each ground target with the same pixel. First, each image is split to select a single sub-swath and to resize the image to conform with the borders of the study area.

Table 1 Input data properties

Satellite	Master image	Slave image	Sub-swath	Orbit pass	Polarization
S1A	05.11.2016	12.11.2017	IW1–IW2–IW3	Descending	VV
S1A	12.11.2017	26.10.2018	IW1–IW2–IW3	Descending	VV
S1A	26.10.2018	14.11.2019	IW1–IW2–IW3	Descending	VV

A

Sentinel 1A
SLC IWx

↓

S1 TOPS Split

↓

S1 Master Image / S1 Slave Image

↓   ↓

Apply Orbit File / Apply Orbit File

↓   ↓

Back-Geocoding

↓

Enhanced Spectral Diversity

↓

Interferogram

↓

TOPSAR-Deburst

↓

Phase &Coherance Map

B

Phase & Coherance Map

↓

Topo Phase Remove

↓

Multilook

↓

Phase Filtering → Snaphu Export → Snaphu Unwrapped → Unwrapped Phase Map

↓

DinSAR

C

DinSAR / Unwrapped Phase Map

↓   ↓

Snaphu Import

↓

Phase to Displacment

↓

Terrain Corection

↓

Displacement Map IWX

Fig. 5 The workflow of the methodology. **A** is the first step is used to complete coregistration. **B** is the second step used to produce DInSAR and the unwrapped phase. **C** is the third step to produce the displacement map

To do a precise orbit correction, apply-orbit-file and back-geocoding coregistration is then implemented with the assistance of a digital elevation map (DEM), the product of the shuttle radar topography mission (SRTM) 3Sec. The next step of coregistration is enhanced spectral diversity (ESD) which is used for the retrieval of the fine azimuth coregistration accuracy (Yague-Martinez et al. 2016). ESD technique estimates the coregistration error more precisely using the burst overlap region (Prats-Iraola et al. 2012). The next step is calculating the interferogram by combining the phases of two coregistrated images.

The interferometric phase of the image pixels is based on the differences between each of the travel paths of these two images according to the resolution cell (Veci 2015). The stack of the results includes the interferometric phase and coherence bands. All burst data are joined by TOPS deburst tool. As original images contain speckle noise, multi-looking process is applied to the next step so that speckled appearance is corrected, and image interpretability is improved (Veci 2015). Before continuing with Snaphu unwrapping, the Goldstein phase filtering operation is performed to reduce the residue on the phase unwrapping

period and to prevent the interferometric phase from temporal decorrelation, geometric decorrelation, volume scattering, and processing error (Veci 2015). Snaphu is an implementation of the statistical-cost, network-flow algorithm for phase unwrapping (Zan et al 2015; Chen and Zebker 2000, 2001). As a result of the second step, the DInSAR phase and unwrapped phase map are obtained. In the third step, DInSAR stack and the unwrapped phase map are assigned as input variables in SNAP software. The last operation to correct the geometric effects of SAR distortions is terrain correction using DEM. The final displacement map is constructed using uplift and subsidence information. The study area includes IW1, IW2, and IW3. Those three steps are implemented for all needed swaths, the swaths are merged as a mosaic and clipped at the study area boundaries.

The coordination of information on the environment (CORINE) 2018 land cover classification data is used to interpret the 3-year displacement map together with land cover classification. CORINE land cover is a program of the European Commission, which was established to create a standardized set of data based on a geographical information system using information about the environment within the European Community. The program has land cover data for the years 1990, 2000, 2006, 2012, and 2018. The data is vector based and includes 44 classes, which have information about land cover and land use classes. These classes have a hierarchical structure and have three levels of classification. The first level data, which are used for this study,

was created from 1/5,00,000 to 1/10,00,000 and lower scales (CORINE Land and Cover 2020).

The data from Sentinel 1A SLC IWx for the years 2016–2019 were used to calculate vertical displacement with differential interferometry of the Konya Plain, referred to as the study area. The result maps of vertical displacement cover the complete IW sub-swats as mosaics for each year separately. Then the final displacement map was created using the raster sum operation (Fig. 6). The CORINE land cover data were used to maintain the vertical displacement based on land use properties. The CORINE land cover data and final vertical displacement results are used together for the flow chart shown in Fig. 12.

Results and discussion

Radar images captured between 2016 and 2019 from Sentinel 1A by the SLC mission and using IWx mode are used to calculate the vertical displacement of Konya Plain with the differential interferometry method. The resulting map of vertical displacement covers the complete IW sub-swats as mosaics. Figure 7 shows the digital elevation map of the Konya region and the extent of the Sentinel-1 frame of subswats (IW1, IW2 and IW3) used in this study.

To observe the relationship between groundwater level and subsidence values reached by remote sensing approach, piezometric maps are created according to groundwater analysis well records taken from the General Directorate of

Fig. 6 Comparative process results between vertical displacement and land cover properties. The results are expressed as a percentage as tabular data
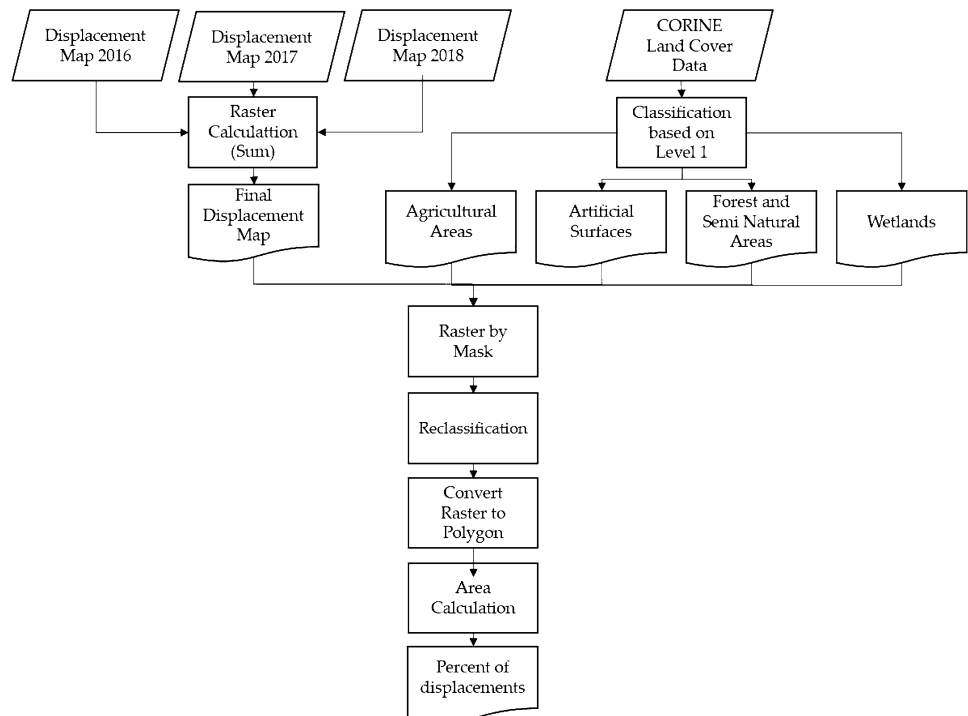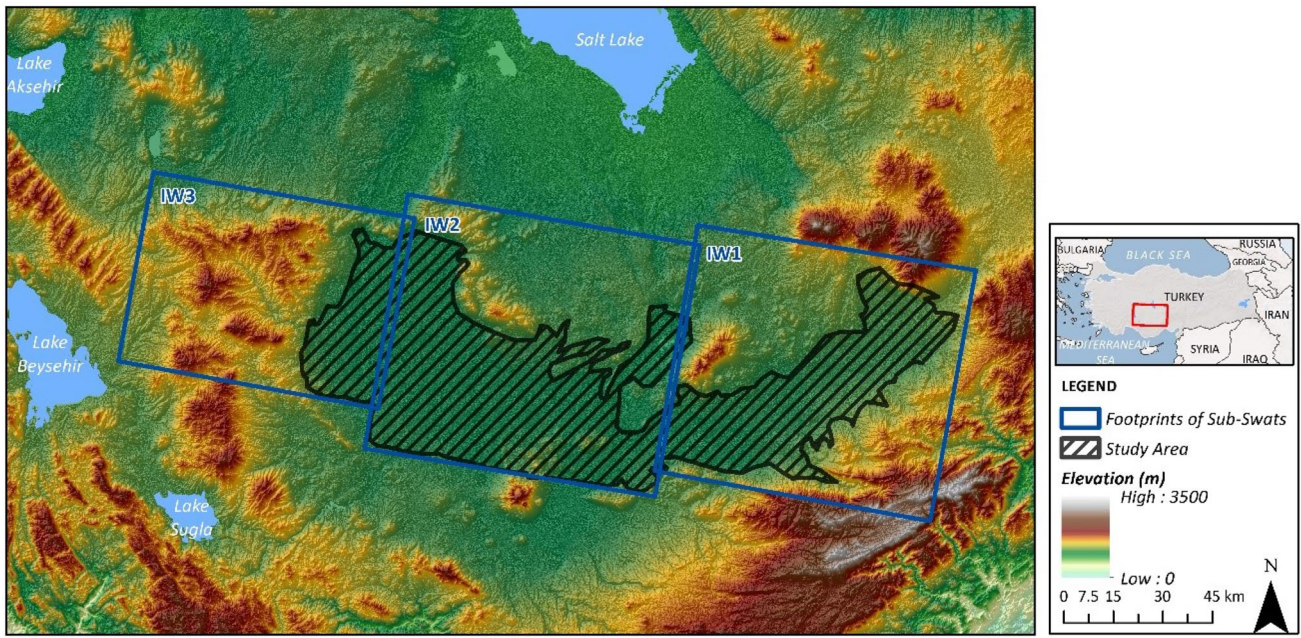
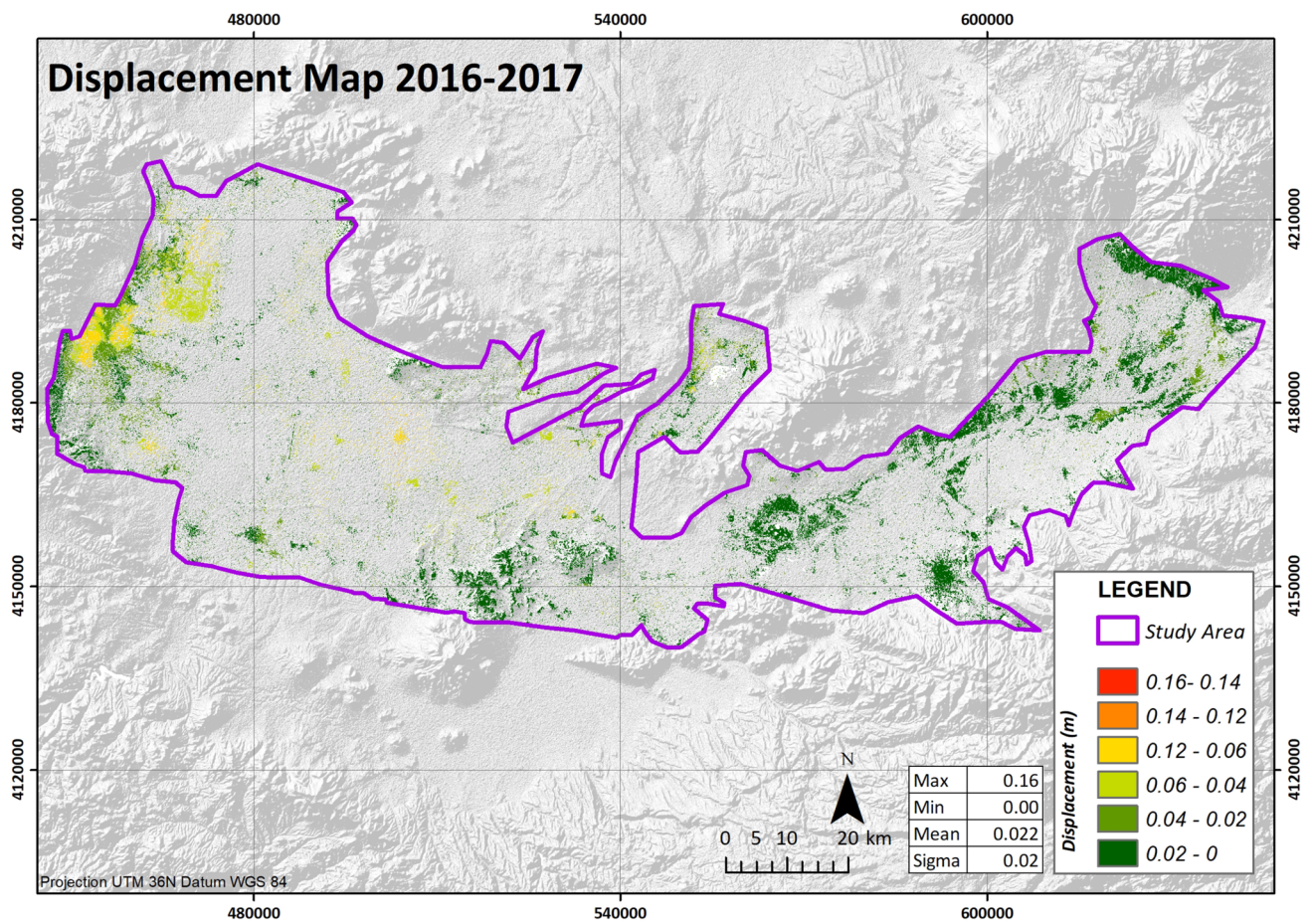**Fig. 7** Elevation map of study area

Fig. 8 Vertical displacement results of years 2016–2017 with 30 m resolution and SRTM 1arc base map

State Hydraulic Works of Turkey (Fig. 4). When groundwater level and subsidence maps are compared, it can be assumed that the low-groundwater level in the northwestern and central part of the study area correlate with subsidence anomalies calculated in the same areas, which affirms our preliminary hypothesis about the reasons for land subsidence (Figs. 8, 9, 10).

The sum of the 3 period of land subsidence is visualized in Fig. 11. From 2016 to 2019, the maximum vertical subsidence was 16 cm. The vertical displacement was evaluated and classified with CORINE land cover classification according to displacement ranges. The land cover was divided into four main classes based on CORINE level 1 as agricultural areas, artificial surfaces, forest and semi natural areas and wetlands (Fig. 12). Then, the vertical displacement and land cover properties are overlaid to evaluate subsidence based on land usage. The overlay results are summed up in Table 2.

The dominant vertical displacement is 0–3 cm for each land cover type. Forest and semi natural areas have their maximum vertical displacement at 3–6 cm, more than the other three classes. The difference between 10 and 15 cm is more dominant on the artificial surfaces. Wetlands generally have 0–3 cm vertical displacement.

The main scope of the study is to give information about the Konya Plain's regional subsidence issue from 2016 to 2019 with three periods, with Sentinel 1 SAR images in a SNAP software environment and from hydrogeological investigations. The aim is to connect the relationship between land subsidence and groundwater level decrease. Both the data and the software were open source, which makes this methodology largely applicable and open to further development for remote sensing applications. The DInSAR method is applied to high accuracy Sentinel 1 SLC IW products. Piezometric, geological and hydrogeological maps are created in ArcMap environments. The hydrogeological data are taken from the General Directorate of State Hydraulic Works of Turkey. Although data from 1968 is considerably weaker than that from 2018, the final piezometric maps provided general information about the groundwater flow and levels.
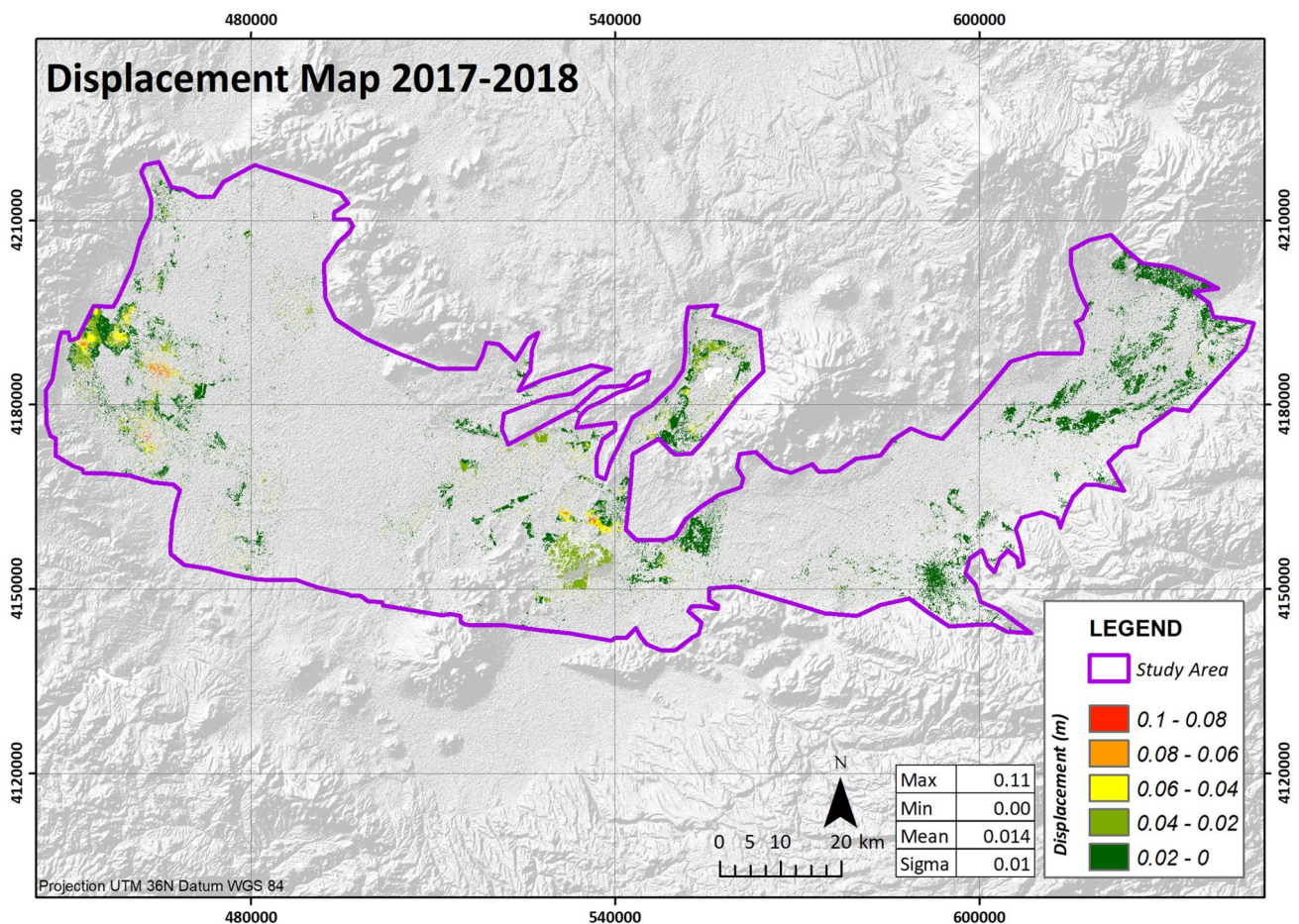

Fig. 9 Vertical displacement results of years 2017–2018 with 30 m resolution and SRTM 1arc base map
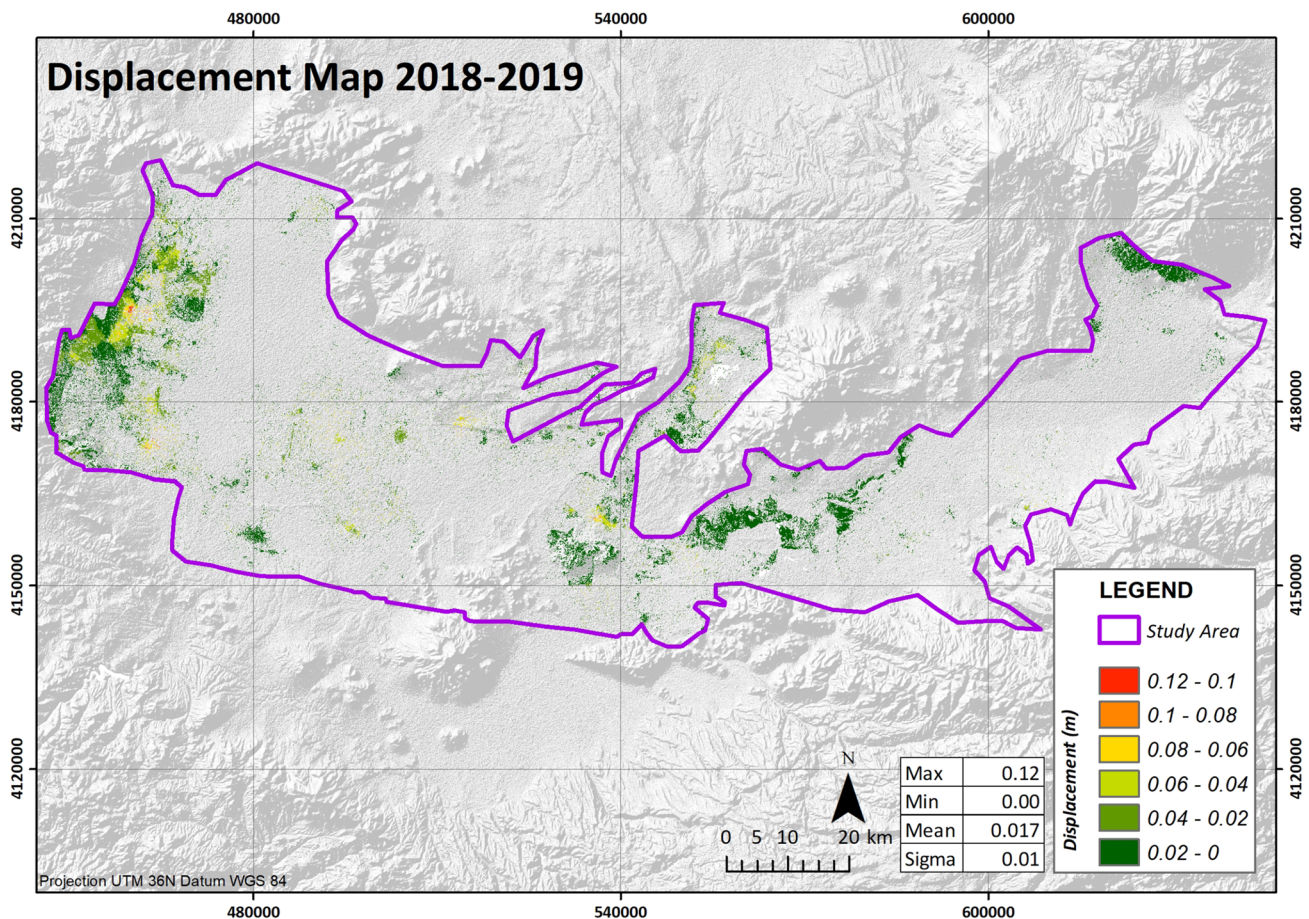
Fig. 10 Vertical displacement results of years 2018–2019 with 30 m resolution and SRTM 1arc base map

The subsidence rate of the Konya Plain was studied by assigning Sentinel-1 satellite radar images to ESA's open-source software, SNAP. The study area exhibits local subsidence spots which are meter to decimeter sized sinkhole and doline structures. The predominant cause of the phenomena is thought to be excess groundwater extraction, which draws attention to land subsidence studies on the Konya Plain. This study aims to come up with a regional explanation for subsidence and a subsidence map.

The relevance of land subsidence is that it affects the daily life of local communities, especially since it has become a fairly frequent natural phenomena caused by excess groundwater extraction over the last few decades. Local collapse, known as Obruk, when happening suddenly or land subsidence of a large area with small displacements every year can be hazardous.

The main aim of land subsidence studies is to calculate the vertical subsidence using SAR products, and to achieve an accuracy from meters to millimeters. For 2016, ground water measurements and calculations, which are based on the study of Özyurt et al. 2018, are taken as the reference point for a comparative point of view. The capacity of

the aquifers was damaged because of the reverse relation between land subsidence and the hydraulic head (Fig. 13). During analysis, the subsidence groundwater system should be taken into consideration. A conceptual model of the aquifer system, groundwater flow model and hydraulic head measurements are taken as reference points. Although final subsidence rates are not equal for each study, a strong correlation can be observed between groundwater level decline and land subsidence rate increment at the northern and western borders of the study area in both SAR image analysis, and hydrogeological conceptualization. This correlation exhibits a consistent temporal gradation with small variations (Fig. 13).

In some parts, however, the maximum values of subsidence rates vary from 0 to 16 cm for different years, points of maximum subsidence can be observed in different regions based on years. Land classification can help us to understand the reason behind the intense land subsidence. As observed in the CORINE land cover map, areas subject to relatively higher land subsidence rates correspond to artificial and agricultural lands, which explains the relationship between groundwater extractions and land subsidence. Despite the
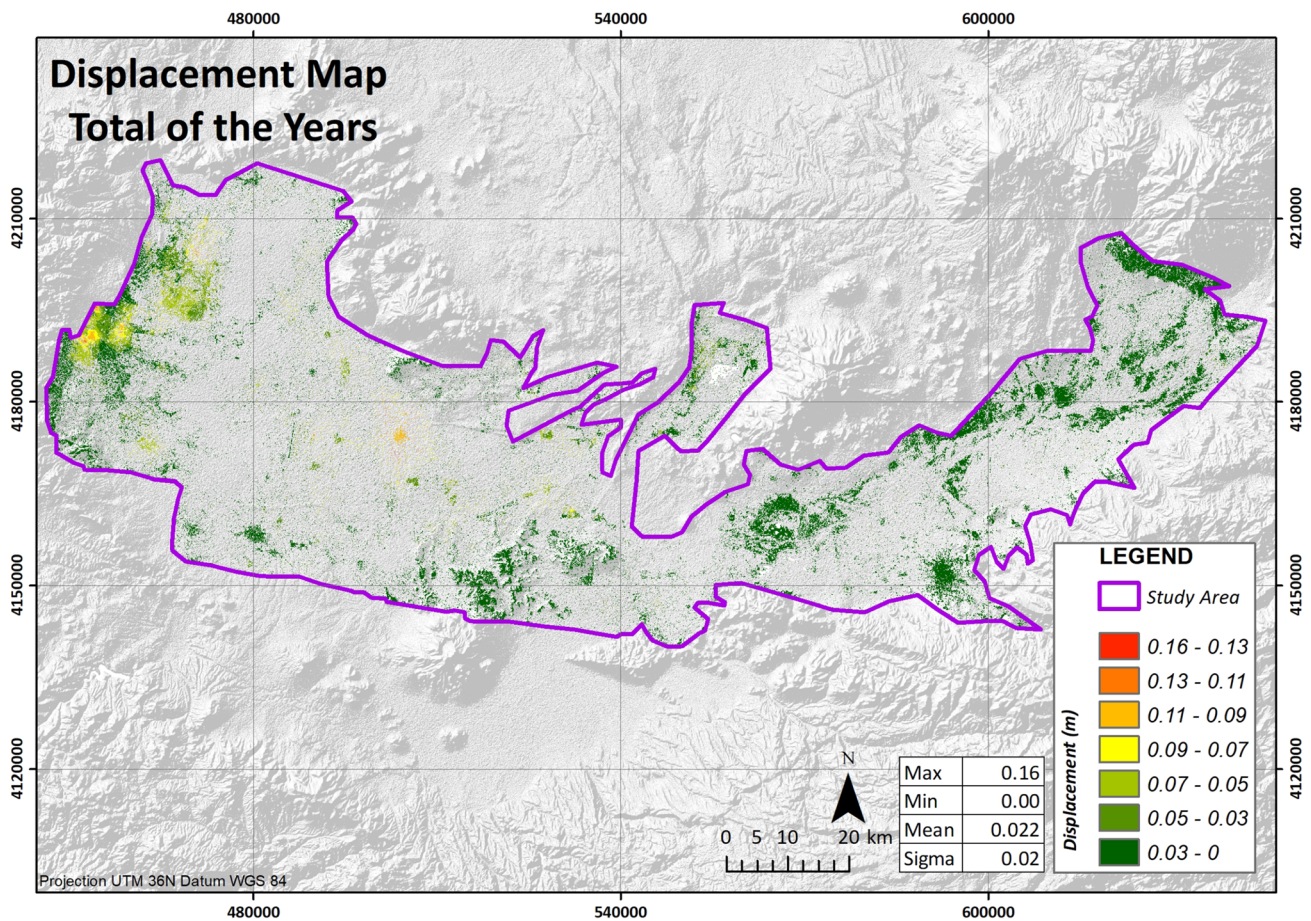
Fig. 11 Vertical displacement results of sum of 2016–2017, 2017–2018 and 2018–2019 with 30 m resolution and SRTM 1arc base map

correlation explained above, occasionally the land subsidence rate does not follow a linear correlation, even if groundwater level follows a linearly decreasing tendency. This can be explained by the artificial impacts of human activity or regional uplift, which sometimes shadow the amount of land subsidence found in SAR image analysis. To observe the temporal variations and the reason behind them, a more detailed research approach analyzing monthly radar images could be helpful in future studies.

Conclusion

Remote sensing applications are not groundbreaking tools in understanding the earth's surface, new features for radar imagery are developed continuously to bring a better understanding of earth system changes. Interferometric synthetic aperture radar (SAR) signals carrying phase information are reliable for studies dealing with deformation of the earth. SAR imagery was herein used to gather annual land subsidence rate information. Although remote sensing information has given reliable results so far, coupling radar imagery with

hydrogeological conceptual models and in-situ groundwater measurements is a notable way results were optimized for the present study.

As land subsidence is a continuous and active phenomenon in Konya region, which is thought to be caused mostly by groundwater extraction and land use practices, a straightforward remote sensing centered land subsidence and groundwater monitoring approach is thought to be useful for recent years and future with Sentinel's SAR imagery because of its accessibility advantages. After approval of the results of the study, automatization of the presented methodology might lead a useful tool in understanding the relation between groundwater extraction and land subsidence and a more frequent land subsidence monitoring opportunity.

In the present study, it is observed that the correlation between groundwater extraction and land subsidence was proven with the use of satellite imagery and hydrogeologic investigation simultaneously. Land subsidence rates were found by satellite imagery subject to the areas where groundwater depletion occurs most. The DInSAR method applied to the SAR images showed high accuracy and resolution of land subsidence information. For the period of 2016–2017,
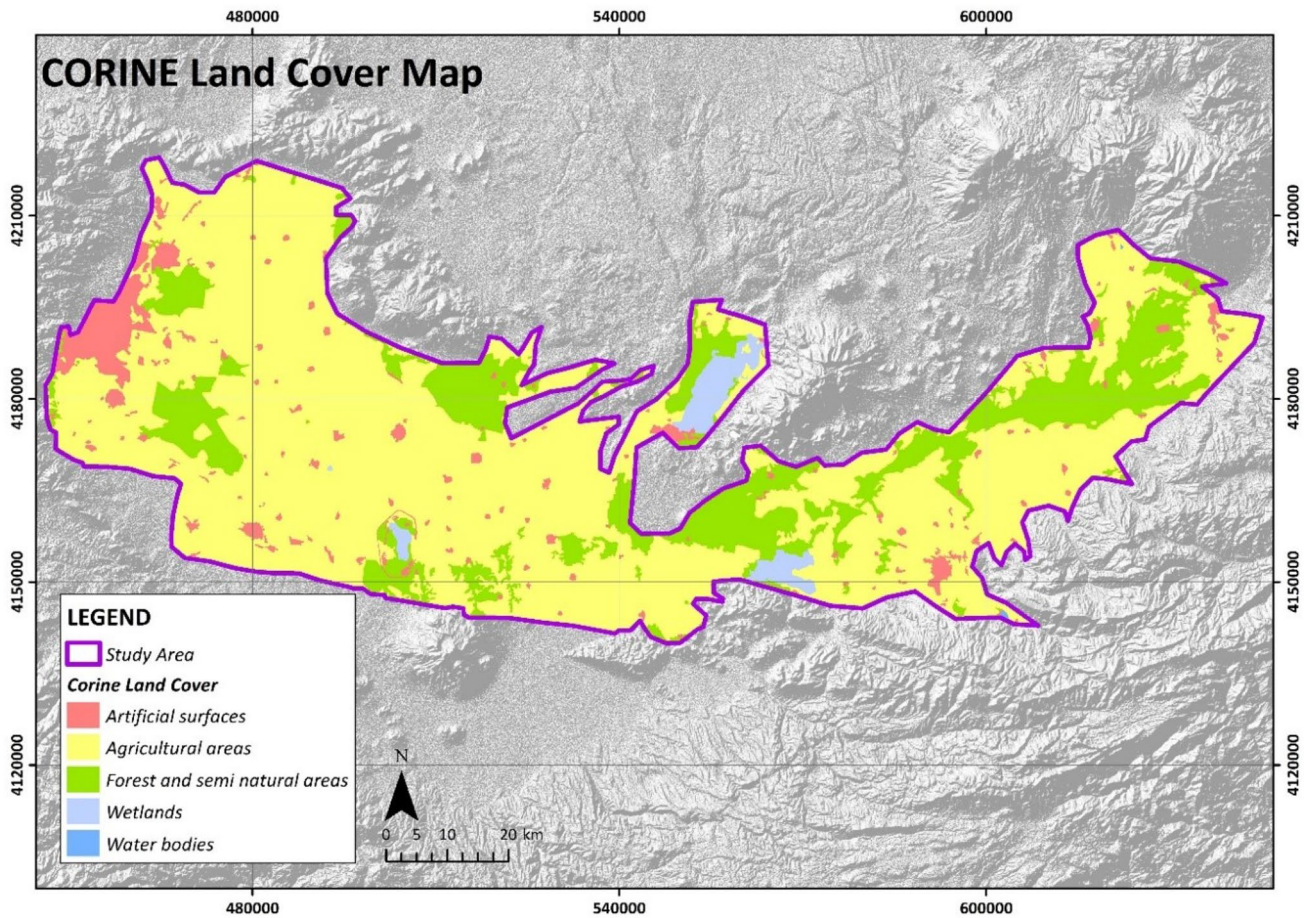
Fig. 12 CORINE land cover classification map of study area

Table 2 Subsidence percentages are based on land cover types

Land cover type	Land subsidence range (m)			
	0.15–0.10 (%)	0.10–0.06 (%)	0.06–0.03 (%)	0.03–0 (%)
Agricultural areas	0.40	2.71	15.28	81.62
Artificial surfaces	1.25	6.19	18.69	73.87
Forest and semi natural areas	0.00	0.72	10.42	88.86
Wetlands	0.00	0.00	10.05	89.95
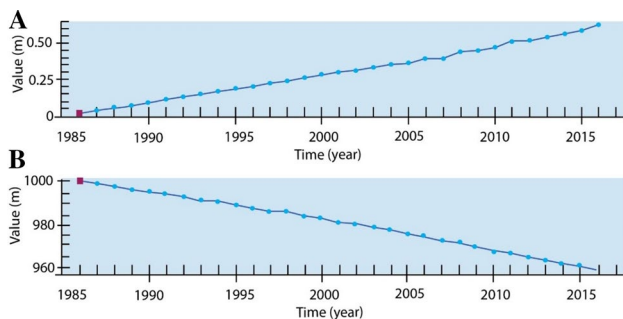
Fig. 13 A Land subsidence **B** hydraulic head of Cumra, Konya (modified from Özyurt et al. 2018)

2017–2018, and 2018–2019, the mean land subsidence rates were 2.2, 1.4 and 1.7 cm/year, respectively. Considering not only the groundwater decline but also the intense urbanization in certain neighborhoods, it can be concluded that artificial surfaces in the urbanized zones and related groundwater demand are the two cooperative trigger effects for land subsidence in the Konya region. Moreover, there are other reasons of land subsidence, which are more nature based that cause mostly sudden subsidence in land that we should not associate with gradual land subsidence. As we approached the land subsidence phenomena annually (3 years in total), particular uncertainties might be identified in the findings

which would be eliminated by a longer period of study and using higher temporal resolution. However, the total land subsidence calculated by satelite imagery for 3 years are more likely to be caused by the long period groundwater decline and increased artifical stress on the ground. Therefore, we could associate the land subsidence with the artifical land cover practices and groundwater extraction over several decades and observe their impact at the present time.

Controlling groundwater extraction limits and enduring DInSAR land subsidence applications for varying time scale spectrums would be an alternative method of observing land subsidence in the Konya plain, and for other regions facing similar problems.

References

Afşin M, Mustafa, Bayari, S, Durukan, U (2012) The origin of carbon dioxide in the groundwater of Konya Closed Basin, central Anatolia, Turkey. https://doi.org/10.13140/2.1.2218.7520

Aksoy R (2019) Extensional neotectonic regime in West-southwest Konya, central Anatolia, Turkey. Int Geol Rev 61:1803–1821. https://doi.org/10.1080/00206814.2019.1581996

Bayari CS, Ozyurt NN, Kilani S (2008a) Radiocarbon age distribution of groundwater in the Konya Closed Basin, central Anatolia, Turkey. Hydrogeol J 17:347–365. https://doi.org/10.1007/s10040-008-0358-2

Bayari CS, Pekkan E, Ozyurt NN (2008b) Obruks, as giant collapse dolines caused by hypogenic karstification in central Anatolia, Turkey: analysis of likely formation processes. Hydrogeol J 17:327–345. https://doi.org/10.1007/s10040-008-0351-9

Canik B, Çörekçioğlu İ (1985) The formation of sinkholes (Obruk) between Karapinar and Kizoren—Konya. Karst water resources (proceedings of the Ankara—Antalya symposium), 161:193–205

Carbognin L, Teatini P, Tosi L (2004) Eustacy and land subsidence in the Venice lagoon at the beginning of the new millennium. J Mar Syst 51:345–353. https://doi.org/10.1016/j.jmarsys.2004.05.021

Chen CW, Zebker HA (2000) Network approaches to two-dimensional phase unwrapping: intractability and two new algorithms. J Opt Soc Am A 17:401. https://doi.org/10.1364/josaa.17.000401

Chen CW, Zebker HA (2001) Two-dimensional phase unwrapping with use of statistical models for cost functions in nonlinear optimization. J Opt Soc Am A 18:338. https://doi.org/10.1364/josaa.18.000338

Chen CW, Zebker HA (2002) Phase unwrapping for large SAR interferograms: statistical segmentation and generalized network models. IEEE Trans Geosci Remote Sens 40:1709–1719. https://doi.org/10.1109/tgrs.2002.802453

Cigna F, Sowter A, Jordan CJ, Rawlins B (2014) Intermittent small baseline subset (ISBAS) monitoring of land covers unfavourable for conventional C-band InSAR: proof-of-concept for peatland environments in North Wales, UK. Remote Sens. https://doi.org/10.1117/122067604

Crosetto M, Crippa B, Biescas E (2005) Early detection and in-depth analysis of deformation by radar interferometry. Eng Geol 79:81–91

Çomut FC, Ustun A, Lazecky M, Perissin D (2016) Capability of detecting rapid subsidence with Cosmo SkyMed and Sentinel-1 dataset over Konya city. Living planet symposium, proceedings of the conference

CORINE Land Cover. In: copernicus. https://land.copernicus.eu/pan-european/corine-land-cover. Accessed 19 Mar 2020

Data products. In: ESA. https://www.esa.int/Our_Activities/Observing_the_Earth/Copernicus/Sentinel-1/Data_products. Accessed 19 Mar 2020

Dirik K, Göncüoglu MC (1996) Neotectonic characteristics of central Anatolia. Int Geol Rev 38(9):807–817. https://doi.org/10.1080/00206819709465363

Doğan U, Yılmaz M (2011) Natural and induced sinkholes of the Obruk plateau and Karapınar–Hotamış plain, Turkey. J Asian Earth Sci 40:496–508. https://doi.org/10.1016/j.jseaes.2010.09.014

Doğdu MŞ, Toklu MM, Sağnak, C (2007) Konya kapalı havzası'nda yağış ve yeraltı suyu değerlerinin irdelenmesi. I. Türkiye İklim Değişikliği Kongresi proceedings, 394–402

Elachi C, Bicknell T, Jordan RL, Wu C (1982) Spaceborne synthetic-aperture imaging radars: applications, techniques, and technology. Proc IEEE 70(10):1174–1209. https://doi.org/10.1109/PROC.1982.12448

Ferretti A, Monti-Guarnieri A, Prati C, Rocca F (2007) InSAR principles: guidelines for SAR interferometry: processing and interpretation. ESA Publications, Noordwijk

Guccione P (2006) Interferometry with ENVISAT wide swath Scan-SAR data. IEEE Geosci Remote Sens Lett 3(3):37–382

Holzer T, Johnson A (1985) Land subsidence caused by ground water withdrawal in urban areas. GeoJournal. https://doi.org/10.1007/bf00186338

Imamoglu M, Kahraman F, Cakir Z, Sanli FB (2019) Ground deformation analysis of Bolvadin (W. Turkey) by means of multi-temporal InSAR techniques and Sentinel-1 data. Remote Sens 11:1069. https://doi.org/10.3390/rs11091069

Kocyigit A (2005) The Denizli graben-horst system and the eastern limit of western Anatolian continental extension: basin fill, structure, deformational mode, throw amount and episodic evolutionary history, SW Turkey. Geodin Acta 18:167–208. https://doi.org/10.3166/ga.18.167-208

Kontogianni V, Pytharouli S, Stiros S (2006) Ground subsidence, quaternary faults and vulnerability of utilities and transportation networks in Thessaly, Greece. Environ Geol 52:1085–1095. https://doi.org/10.1007/s00254-006-0548-y

Lofgren BE (1969) Land subsidence due to the application of water. In: Varnes DJ, Kiersch G (eds) Reviews in engineering geology. Geological Society of America, United States of America

Motagh M, Djamour Y, Walter TR et al (2007) Land subsidence in Mashhad valley, northeast Iran: results from InSAR, levelling and GPS. Geophys J Int 168:518–526. https://doi.org/10.1111/j.1365-246x.2006.03246.x

Okay AI, Tüysüz O (1999) Tethyan sutures of northern Turkey. Geol Soc Lond Spec Pub 156:475–515. https://doi.org/10.1144/gsl.sp.1999.156.01.22

Osmanoglu B, Sunar F, Wdowinski S, Cabral-Cano E (2015) Time series analysis of InSAR data: methods and trends. ISPRS J

Photogramm Remote Sens. https://doi.org/10.1016/j.isprsjprs.2015.10.003

Ozdemir A (2015) Investigation of sinkholes spatial distribution using the weights of evidence method and GIS in the vicinity of Karapinar (Konya, Turkey). Geomorphology 245:40–50. https://doi.org/10.1016/j.geomorph.2015.04.034

Özyurt NN, Avcı P, Bayarı CS (2018) Using groundwater flow modelling for investigation of land subsidence in the Konya closed basin (Turkey). In: Ceryan N (ed) Handbook of research on trends and digital advances in engineering geology. United States of America, IGI Global, pp 569–590. https://doi.org/10.4018/978-1-5225-2709-1.ch016

Perski Z (2003) InSAR and POLinSAR for land subsidence monitoring—user perspective. Applications of SAR polarimetry and polarimetric interferometry. France, Europe Space Agency, pp 321–326

Prats-Iraola P, Scheiber R, Marotti L et al (2012) TOPS interferometry with TerraSAR-X. IEEE Trans Geosci Remote Sens 50:3179–3188. https://doi.org/10.1109/tgrs.2011.2178247

Schubert AD, Small N, Miranda D, Geudtner D, Meier E (2015) Sentinel-1a product geolocation accuracy: commissioning phase results. Remote Sens 7(7):9431–9449

Sowter A, Bateson L, Strange P, Ambrose K, Moh FS (2013) DInSAR estimation of land motion using intermittent coherence with application to the south Derbyshire and Leicestershire coalfields. Remote Sens Lett 4(10):979–987. https://doi.org/10.1080/2150704X.2013.823673

Teatini P, Ferronato M, Gambolati G et al (2005) A century of land subsidence in Ravenna, Italy. Environ Geol 47:831–846. https://doi.org/10.1007/s00254-004-1215-9

Teatini P, Ferronato M, Gambolati G, Gonella M (2006) Groundwater pumping and land subsidence in Emilia-Romagna coastland, Italy: modeling the past occurrence and the future trend. Water Resour Res. https://doi.org/10.1029/2005wr004242

Jiang T-C, Li T, Liu J-N (2011) Research on deformation monitoring caused by large earthquake with WSM interferometry Proc. SPIE 8286, International symposium on lidar and radar mapping, technologies and applications, 82861N. https://doi.org/10.1117/12.912465

Potin P et al. (2015) Sentinel-1 mission status, in 2015 IEEE international geoscience and remote sensing symposium (IGARSS), pp 2820–2823, Milan: IEEE. https://doi.org/10.1109/IGARSS.2015.7326401

User guides—Sentinel-1 SAR—revisit and coverage—Sentinel online. In: Sentinel. https://sentinel.esa.int/web/sentinel/user-guides/sentinel-1-sar/revisit-and-coverage. Accessed 19 Mar 2020

Ustun A, Tusat E, Yalvac S (2010) Preliminary results of land subsidence monitoring project in Konya Closed Basin between 2006–2009 by means of GNSS observations. Nat Hazards Earth Syst Sci 10:1151–1157. https://doi.org/10.5194/nhess-10-1151-2010

Üstün A, Tuşat E, Yalvaç S et al (2015) Land subsidence in Konya Closed Basin and its spatio-temporal detection by GPS and DInSAR. Environ Earth Sci 73:6691–6703. https://doi.org/10.1007/s12665-014-3890-5

Veci L (2015) Sentinel-1 Toolbox: TOPS interferometry tutorial; Array Systems Computing Inc

Widodo J, Herlambang A, Sulaiman A et al (2019) Land subsidence rate analysis of Jakarta metropolitan region based on D-InSAR processing of Sentinel data C-band frequency. J Phys Conf Ser 1185:012004. https://doi.org/10.1088/1742-6596/1185/1/012004

Xue Y-Q, Zhang Y, Ye S-J et al (2005) Land subsidence in China. Environ Geol 48:713–720. https://doi.org/10.1007/s00254-005-0010-6

Yague-Martinez N, Prats-Iraola P, Gonzalez FR et al (2016) Interferometric processing of Sentinel-1 TOPS data. IEEE Trans Geosci Remote Sens 54:2220–2234. https://doi.org/10.1109/tgrs.2015.2497902

Yilmaz M (2010) Environmental problems caused by ground water level changes around Karapinar. Ankara Üniversitesi Çevre Bilimleri Dergisi 2(2):145–163

Zan FD, Guarnieri AM (2006) TOPSAR: terrain observation by progressive scans. IEEE Trans Geosci Remote Sens 44:2352–2360. https://doi.org/10.1109/tgrs.2006.873853

Zan FD, Prats-Iraola P, Rodriguez-Cassola M (2015) On the dependence of delta-k efficiency on multilooking. Geosci Remote Sens Lett 12:1745–1749. https://doi.org/10.1109/lgrs.2015.2424272